Science and Innovation of Advanced Materials

The Materials Research Society of Thailand

Research Article

Co-precipitation Synthesis and Characterization Studies of Manganese Oxide Doped with Nickel for High-Performance Energy Storage Supercapacitor Application

Rattanapat Jareanwat*, Asanee Somdee, Surangkana Wanapop

Faculty of Science, Energy, and Environment, King Mongkut's University of Technology North Bangkok Rayong Campus, Rayong 21120, Thailand

* Corresponding author e-mail: s6513021856017@email.kmutnb.ac.th

Received: *May 12th, 2024* | ***Revised:*** *August 20th, 2024* | ***Accepted:*** *August 27th, 2024*

Abstract: The advancement in nanotechnology research has facilitated the development of eco-friendly methods for the synthesis of nanoparticles. In this work, nickel (Ni)-doped manganese oxide was synthesized using the co-precipitation method. The prepared Ni-doped manganese oxide products have been characterized by X-ray powder diffraction, scanning electron microscopy (SEM), transmission electron microscope (TEM), and energy dispersive X-ray spectroscopy (EDS). The preliminary electrochemical characteristics include charge-discharge cycling, which improves the conductivity and capacitance of the high-performance aqueous asymmetrical supercapacitor. The CV analysis of the Ni-doped manganese oxide electrode demonstrated a distinctive pseudocapacitive behavior in 1 M KOH solution. The nickel (Ni) doped electrode has a higher specific capacitance value than the pure manganese oxide electrode, with a value of 2225.07 $F \cdot g^{-1}$ at a scan rate of 5 $mV \cdot s^{-1}$.

Keywords: Supercapacitor, Co-precipitation method, Nanotechnology, Synthesized, Electrochemical

1. Introduction

Nowadays, many tremendous efforts and research focus on clean, renewable energy resources and energy storage systems due to the looming scarcity of fossil fuels and growing ecological concerns. Due to the fast growth of the universal economy, a high energy demand requires new energy technology to fulfill world development needs. To solve this crisis, recent research on energy conversion and storage, such as lithium-ion batteries, sodium ions, metal-air, fuel cells, and supercapacitors, has become an eminent research topic [1-3].

Supercapacitors are electrochemical energy storage devices catching more attention due to their elevated good stability, high electrical power density, low-cost production, long cycling stability, non-hazardous to the environment, and other excellent properties [4]. Supercapacitors can be divided into pseudocapacitors (PCs) and electric double-layer capacitors (EDLCs). EDLCs cover conductive porous carbon composite materials, such as graphene, super carbon, and activated carbon (AC) [5,6]. Specifically, certain metal oxides and low-price hydroxides, such as ZnO, α-Fe_2O_3, MnO_2, Mn_3O_4, and NiO, were researched and reported as potential electrode materials.

* The work was presented at The 22nd International Symposium on Eco-materials Processing and Design (ISEPD 2024), 21-24 January 2024

Manganese oxide nanoparticles have a broad range of applications, including their use as catalysts, molecular sieves, and components in low-cost, environmentally friendly batteries, thanks to their widespread availability [7]. Manganese oxide nanomaterial can be synthesized by various methods such as the hydrothermal method [8], redox method [9], co-precipitation method [10], sol–gel process [11]. Among these preparation methods, the co-precipitation chemical method has more advantages when synthesizing the nanomaterial.

In this work, manganese oxide and Ni-doped manganese oxide nanoparticles were synthesized using the co-precipitation method. The products were characterized by various methods and applied as the supercapacitor electrode materials.

2. Methodology

2.1 Research materials

Manganese(II) acetate tetrahydrate ($(CH_3COO)_2Mn{\cdot}4H_2O$), nickel(II) acetate tetrahydrate ($Ni(CH_3COO)_2{\cdot}4H_2O$), sodium hydroxide (NaOH), ethyl alcohol (CH_3CH_2OH), polyvinylidene fluoride (PVDF), and potassium hydroxide (KOH) with analytical grade quality were purchased from Merck.

2.2 Preparation for un-doped Mn_3O_4/Mn_5O_8 and Ni-doped Mn_3O_4/Mn_5O_8 nanoparticles

The co-precipitation method was used to prepare Mn_3O_4/Mn_5O_8. The typical synthesis process began by dissolving 3 mmol of manganese acetate tetrahydrate ($(CH_3COO)_2Mn{\cdot}4H_2O$) in 60 ml of deionized (DI) water. The solution was stirred at room temperature for 10 minutes. Subsequently, 3 M NaOH was added and the mixture was stirred for 2 hours. The final product was washed with DI water and ethanol and dried at 60 °C for 12 hours. The sample was then calcined at 450 °C for 2 hours, resulting in the formation of Mn_3O_4/Mn_5O_8. Ni-doped Mn_3O_4/Mn_5O_8 was synthesized using the same co-precipitation method as Mn_3O_4/Mn_5O_8, with the addition of 5 wt% $(CH_3COO)_2Mn{\cdot}4H_2O$) during the synthesis process.

2.3 Preparation of working electrode

The electrochemical properties of the synthesized Mn_3O_4/Mn_5O_8 and Ni-doped Mn_3O_4/Mn_5O_8 nanoparticles were evaluated using a working electrode prepared on nickel foam (1×2 cm^2). The process began by thoroughly cleaning the nickel foam. The test materials were then ground together with PVDF and carbon black in a weight ratio of 80:10:10, using NMP as the solvent. The resulting viscous slurry was evenly coated onto the clean nickel foam and subsequently dried in a vacuum oven at 110 °C for 12 hours before electrochemical characterization.

3. Results and discussion

The XRD patterns of Mn_3O_4/Mn_5O_8 and Ni-doped Mn_3O_4/Mn_5O_8 nanoparticles are shown in Figure 1. From the result, the diffraction pattern of un-doped and doped is similar, indicating that the Ni atom is undergoing substitution into the Mn site. The diffraction peaks of Mn_3O_4/Mn_5O_8 at the 2θ angles of 17.96°, 21.60°, 23.75°, 28.92°, 30.96°, 36.09°, 38.24°, 39.26°, 44.35°, 47.74°, 49.21°, 50.80°, 53.83°, 56.08°, 58.43° and 66.17° are well-matched with the standard PDF file Mn_5O_8 (PDF 00-03901218) with monoclinic phase structure where the corresponding mirror plane of diffraction are (200), (-201), (112), (201), (-220), (-221), (002), (221), (022), (600) and (-223), respectively. The peaks at 2θ angles of 17.96°, 28.92°, 30.96°, 32.10°, 36.09°, 38.24°, 44.35°, 50.80°, 53.83°, 56.08°, 58.43°, 59.92°, 64.54°, 74.08°, and 76.51° corresponding to the planes (101), (111), (200), (103), (202), (004), (220), (105), (312), (303), (321), (400), and (422) are well-indexed to the tetragonal phase of Mn_3O_4 (PDF 01-0800 382).

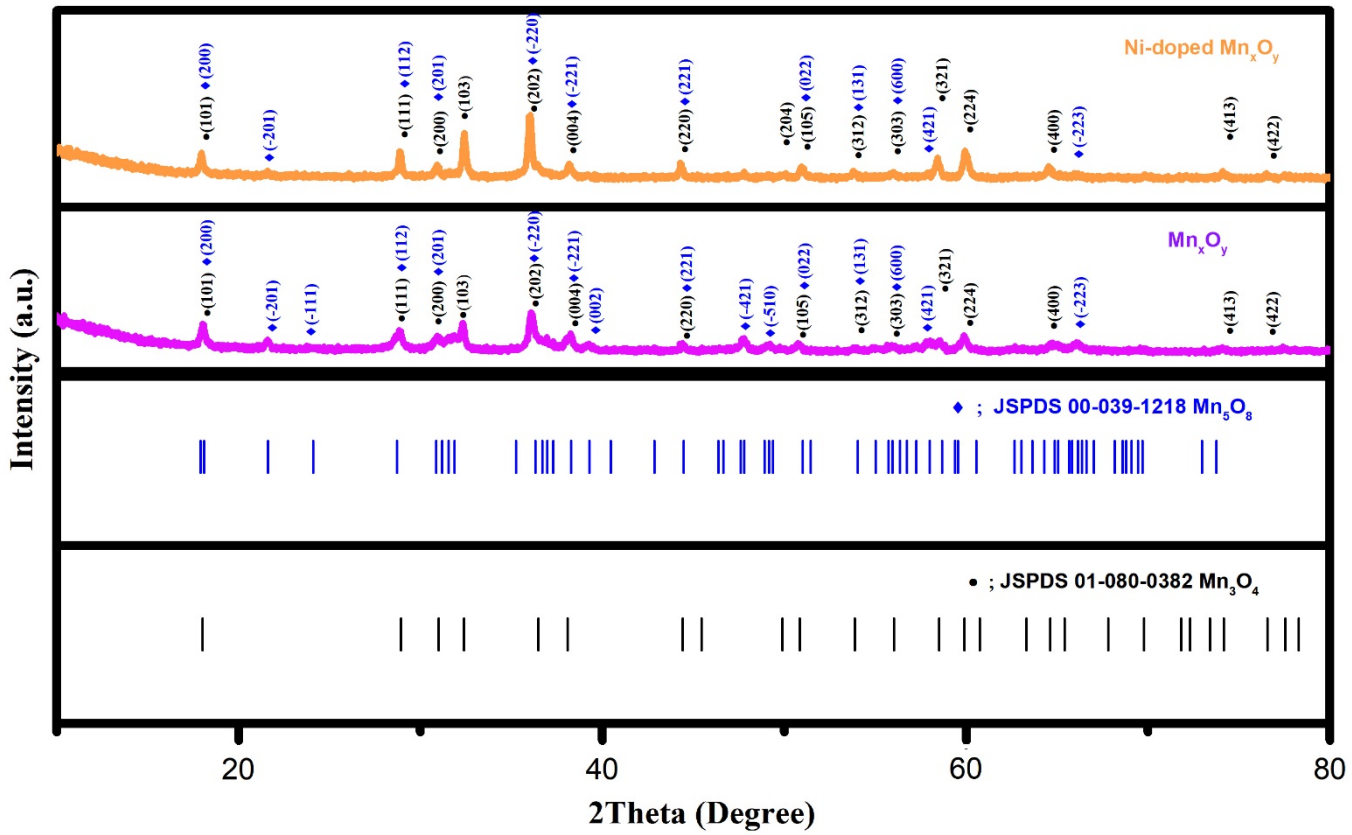

Figure 1 XRD patterns of Mn_3O_4/Mn_5O_8 and Ni-doped Mn_3O_4/Mn_5O_8.

It was also noted that nickel contents affect the crystal structure of Mn_3O_4/Mn_5O_8. Nickel doping promotes the formation of Mn_5O_8 and Mn_3O_4 nanoparticles [12-14]. The Ni doped of Mn_3O_4/Mn_5O_8 peaks at 2θ of 17.96°, 28.91°, 30.91°, 32.45°, 36.07°, 38.15°, 44.24°, 50.95°, 53.88°, 55.95°, 58.42°, 59.96°, 64.58°, 74.07°, and 76.53°, matched with the PDF file Mn_5O_8, correspond to the planes (101), (111), (200), (103), (202), (004), (220), (204), (105), (312), (303), (321), (224), (400), (413), and (422), respectively. The peaks at 2θ of 17.97°, 21.60°, 28.98°, 30.99°, 35.99°, 38.14°, 44.24°, 51.04°, 53.88°, 56.10°, 57.81°, and 66.12°, matched with the PDF file Mn_5O_8, correspond to the planes (200), (-201), (112), (201), (-220), (-221), (221), (022), (131), (600), (421), and (-223), respectively. After doping with Ni, the peaks became more crystalline, with observed peaks at 32.45° and 36.14°. This indicates increased peak intensity due to Ni insertion into the manganese oxide lattice.

As shown in Figure 2, the SEM images of Mn_3O_4/Mn_5O_8 and Ni-doped Mn_3O_4/Mn_5O_8 reveal different morphologies. The powder contains spherical to rod-like nanoparticles as depicted in Figures 2(a) and 2(b). The SEM images show spherical nanoparticle-like structures resulting from nanoparticle agglomeration [15-16]. The change in morphologies was observed for Mn_3O_4/Mn_5O_8 nanoparticles. The significant nanostructure change in the sample is observed by adding Ni-doped Mn_3O_4/Mn_5O_8 nanoparticles. The particle-size diameter of 100 nm compares Figure 2(a) forming bigger than Figure 2(b). The consequence manifests that the Ni-doped Mn_3O_4/Mn_5O_8 can effectively restrain the grans from aggregating in this experiment. This study aimed to understand and analyse surfaces, which contribute to enhancing electrochemical performance of materials. Energy dispersive spectroscopic analysis of Ni-doped Mn_3O_4/Mn_5O_8 confirms the existence of manganese, oxygen, and nickel with weight percentage. Figure 2(c) characterized the material of chemical composition peak of manganese, oxygen, and nickel with few minor elements like carbon and calcium elements. Here, it is clearly shown that the relative atomic abundance of manganese present on the surface. Thus, the excess of manganese atoms, represented in material formation, enhances the agglomeration.

In Figure 2, the energy-dispersive X-ray spectroscopy (EDS) reveals the presence of Mn_3O_4/Mn_5O_8 nanoparticles with atomic weight ratios of manganese, oxygen, and nickel detailed in Table 1.

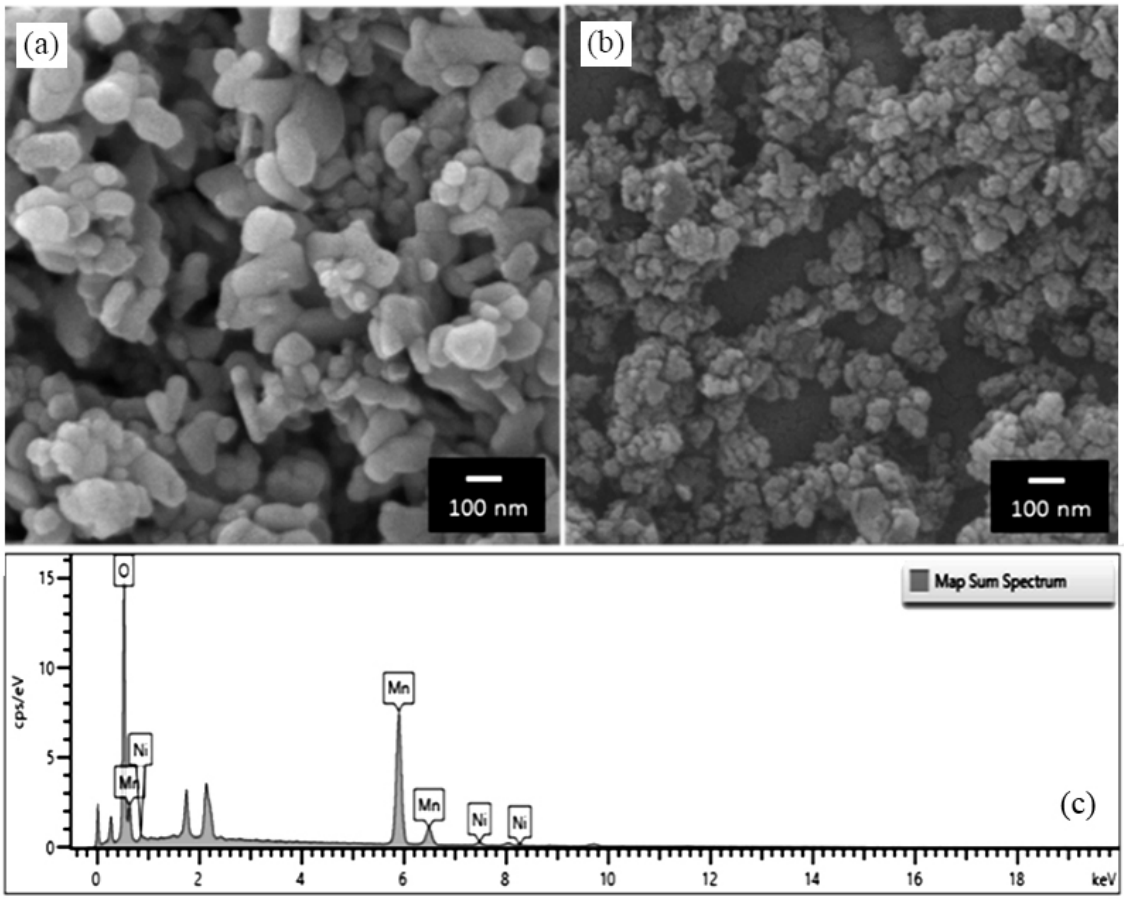

Figure 2 (a) SEM image of Mn_3O_4/Mn_5O_8, (b) SEM image of Ni-doped Mn_3O_4/Mn_5O_8 and (c) EDS of Ni-doped Mn_3O_4/Mn_5O_8.

Table 1 Synthesized Ni-doped manganese oxide nanoparticles of elemental composition

Elements	Line type	wt%	wt% Sigma	Atomic%
O	K series	24.76	0.20	53.11
Mn	K series	72.32	0.27	45.18
Ni	K series	2.93	0.25	1.71
Total		100		100

TEM images of un-doped and Ni-doped Mn_3O_4/Mn_5O_8 are shown in the Figure 3. Figure 3(b) shows a lattice spacing of 0.28 nm, which is specified to the (111) facets, while Figure 3(d) shows a lattice spacing of 0.19 nm belonged to Mn_5O_8 [17-19].

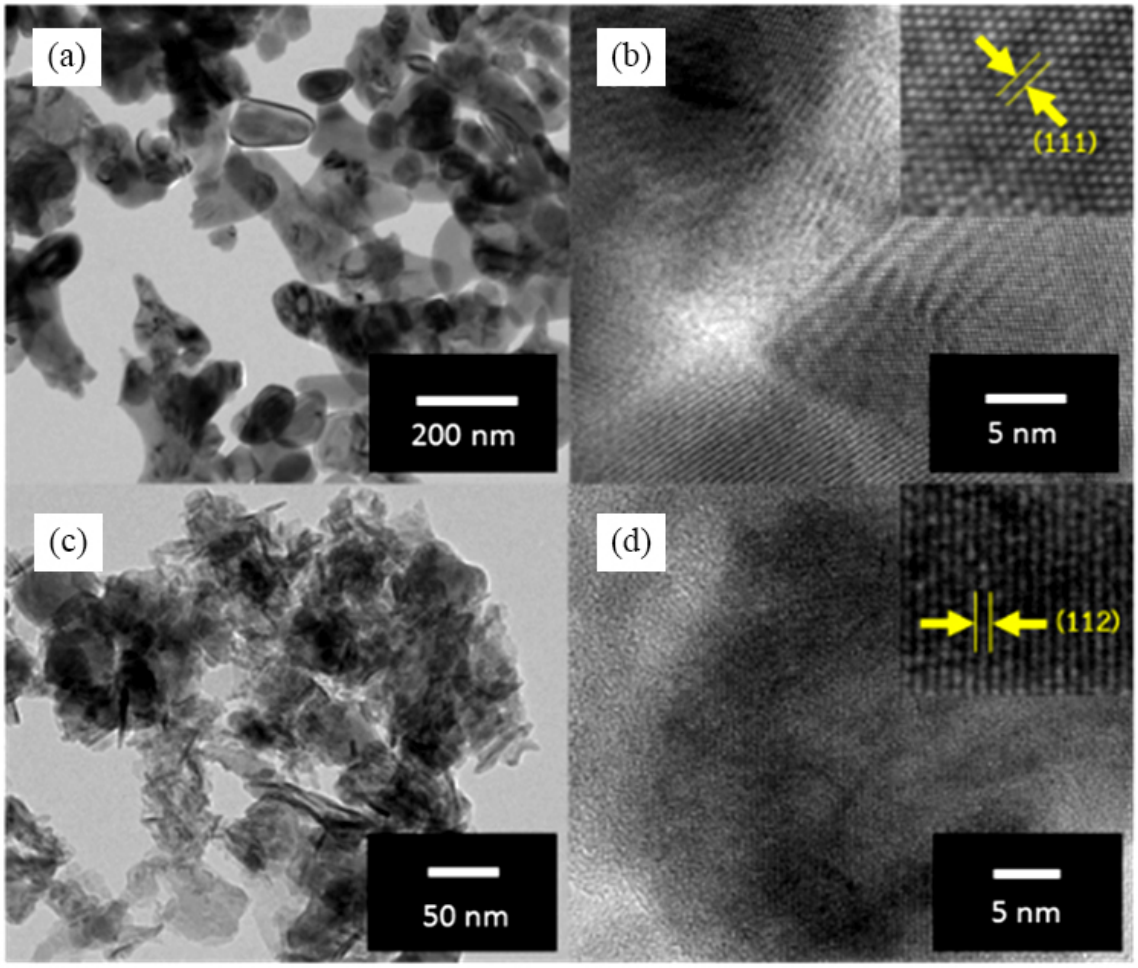

Figure 3 (a) TEM images of Mn_3O_4/Mn_5O_8, (b) HRTEM image of Mn_3O_4/Mn_5O_8, (c) TEM images of Ni-doped Mn_3O_4/Mn_5O_8 and (d) HRTEM image of Ni-doped Mn_3O_4/Mn_5O_8.

The CV curve can directly reflect the electrochemical behavior of the electrode surface in the course of the charge and discharge process. Figure 4(a) shows the CV graph of Mn_3O_4/Mn_5O_8 under the scan rate of 5-100 $mV{\cdot}s^{-1}$.

Figure 4(b) shows a CV curve of Ni-doped Mn_3O_4/Mn_5O_8 under the scan rate of 5-100 $mV{\cdot}s^{-1}$. The integral area enclosed by the CV curve can reflect the specific capacitance of the material. Figure 4(c) compares the un-doped and Ni-doped Mn_3O_4/Mn_5O_8. As clear evidence of the CV curve, the Ni-doped into the Mn_3O_4/Mn_5O_8 showed a larger CV curve, which implied the capacitance increase. Figure 5 shows GCD curves of as-synthesized electrodes of Mn_3O_4/Mn_5O_8 and Ni-doped Mn_3O_4/Mn_5O_8 at an applied charge-discharge current density of 0.1 $mA{\cdot}g^{-1}$ within the potential window 0 to 0.5 (V) in 1 M KOH electrolyte. The nonlinear GCD curves indicate the characteristic pseudocapacitive behavior. The result indicates that the electrode fabricated from Ni-doped Mn_3O_4/Mn_5O_8 electrode shows a higher discharging time than that of Mn_3O_4/Mn_5O_8.

Figure 6 shows the specific capacitance at various scan rates. In this work, the highest capacitance of 2225.71 $F{\cdot}g^{-1}$ was obtained, which is the Ni-doped Mn_3O_4/Mn_5O_8. Furthermore, the comparison of Nyquist plots in Figure 7 shows the well internal resistance within the Ni-doped Mn_3O_4/Mn_5O_8 electrode over the un-doped one. The other values were summarized as shown in the Table 2.

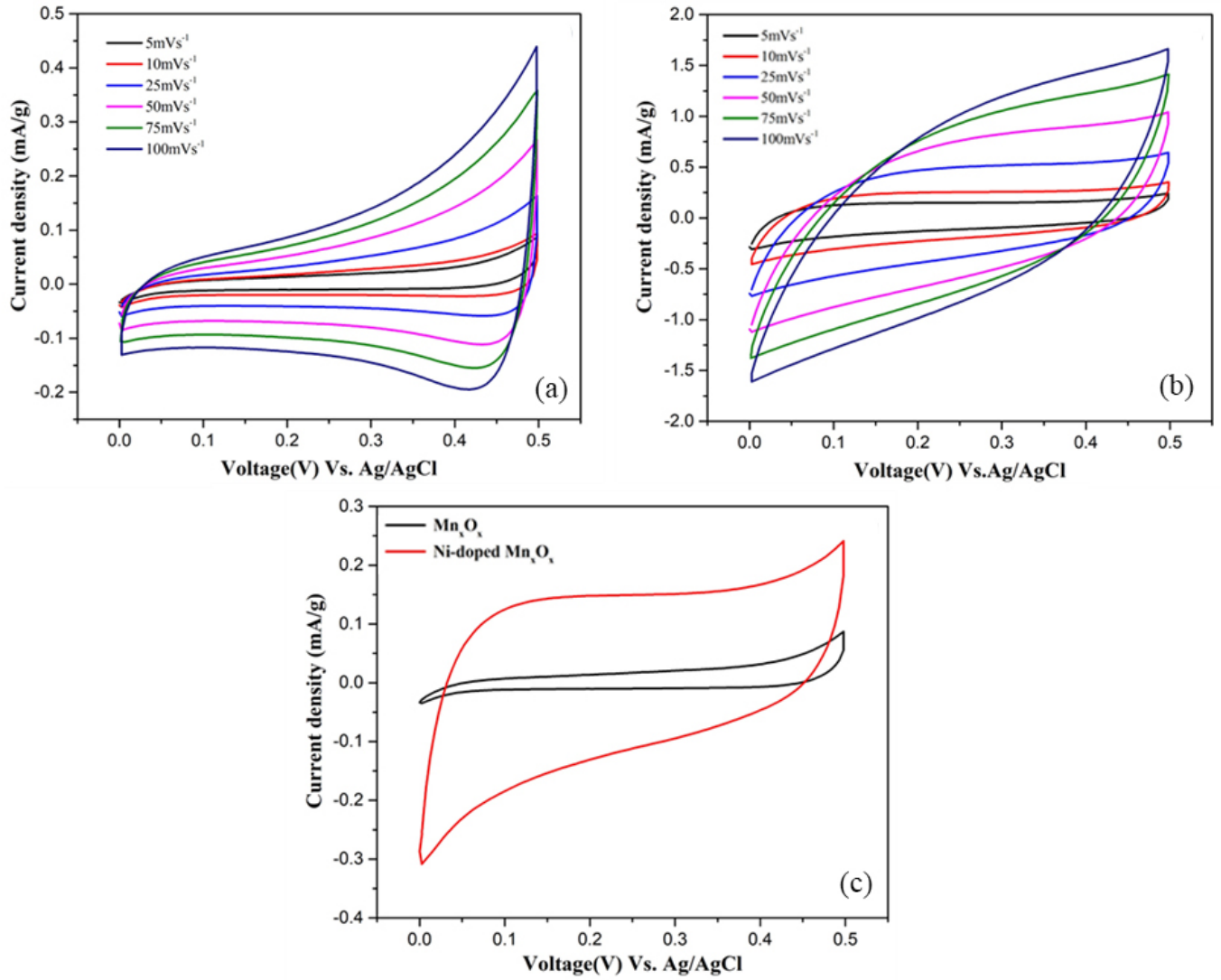

Figure 4 CV curves of sample Mn_3O_4/Mn_5O_8 and Ni-doped Mn_3O_4/Mn_5O_8; (a) CV curve of Mn_3O_4/Mn_5O_8 with the different scanning rates, (b) CV curve of Ni-doped Mn_3O_4/Mn_5O_8 at different scanning rates, (c) CV curve of comparison curve of Mn_3O_4/Mn_5O_8 and Ni-doped Mn_3O_4/Mn_5O_8 at a 5 $mV{\cdot}s^{-1}$ scanning rate.

Table 2 Specific capacitance of Mn_3O_4/Mn_5O_8 and Ni doped Mn_3O_4/Mn_5O_8 with scan rates of 5-100 $mV{\cdot}s^{-1}$

Scan rate ($mV{\cdot}s^{-1}$)	Specific capacitance ($F{\cdot}g^{-1}$)	
	Mn_3O_4/Mn_5O_8	Ni doped Mn_3O_4/Mn_5O_8
5	225.6091	2225.71
10	158.578	1539.508
25	128.912	1123.015
50	109.8689	816.323
75	99.2671	648.333
100	91.794	539.98

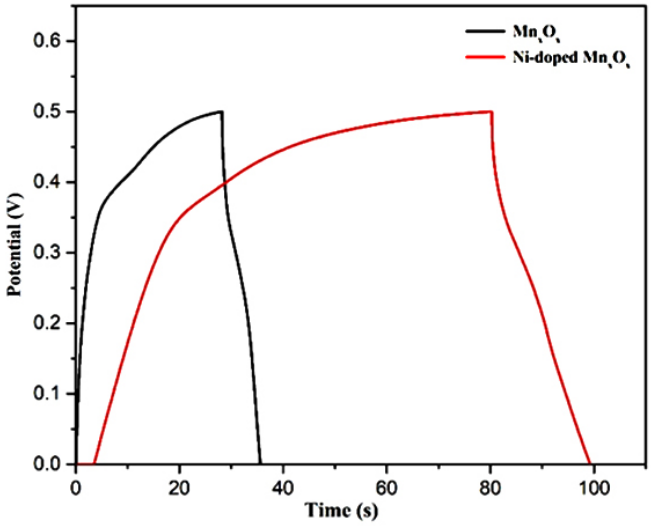

Figure 5 GCD electrode of sample Mn_3O_4/Mn_5O_8 and Ni doped Mn_3O_4/Mn_5O_8 at a current density of 0.1 mA·g^{-1}.

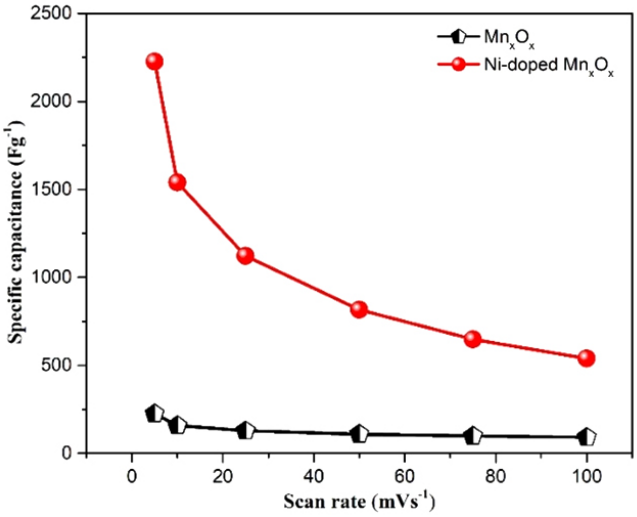

Figure 6 The plot of specific capacitances versus scan rates for Mn_3O_4/Mn_5O_8 and Ni-doped Mn_3O_4/Mn_5O_8.

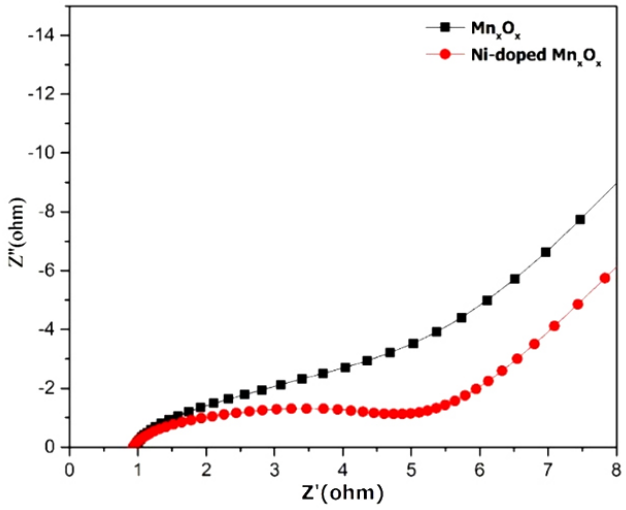

Figure 7 Nyquist plot of Mn_3O_4/Mn_5O_8 and Ni-doped Mn_3O_4/Mn_5O_8.

4. Conclusion

Mn_3O_4/Mn_5O_8 and Ni-doped Mn_3O_4/Mn_5O_8 were studied in this research. The materials were applied as a supercapacitor electrode. The materials were synthesized by employing the co-precipitation method, and the product was characterized by various methods. The performance of Ni-doped Mn_3O_4/Mn_5O_8 is significantly better than the pure one. At a 5 mV·s^{-1} scan rate, the over 2,000 F·g^{-1} of Ni-doped Mn_3O_4/Mn_5O_8 can be obtained. The EIS indicated that the Ni-doped assisted the charge transfer and reduced the internal resistance of the parent Mn_3O_4/Mn_5O_8 to increase efficiency.

Acknowledgment

This research was funded by King Mongkut's University of Technology North Bangkok. Contact no. KMUTNB-66-KNOW-08.

References

[1] K. M. Racik, A. Manikandan, M. Mahendiran, J. Madhavan, M. V. A. Raj, M. G. Mohamed, T. Maiyalagan, Hydrothermal synthesis and characterization studies of α-Fe_2O_3/MnO_2 nanocomposites for energy storage supercapacitor application, *Ceram. Int.* **46** (2020) 6222-6233.

[2] A. M. Tamboli, M. S. Tamboli, S. K. Shinde, J. Byeon, N. T. N. Truong, C. Kim, C. Park, Uniform and fully decorated novel Li-doped α-Fe_2O_3 nanoparticles for high performance supercapacitors, *J. Alloys Compd.* **928** (2022) 167242.

[3] S. A. Al-Ghamdi, A. A. A. Darwish, T. A. Hamdalla, A. Pasha, M. E. Elnair, A. Al-Atawi, S. Khasim, Biological synthesis of novel carbon quantumdots using Halimedaopuntial green algae with improve edoptical properties and electrochemical performance for possible energy storage applications, *Int. J. Electrochem. Sci.* **18** (2023) 100102.

[4] K. Seevakan, A. Manikandan, P. Devendran, Y. Slimani, A. Baykal, T. Alagesan, Structural, morphological and magneto-optical properties of $CuMoO_4$ electrochemical nanocatalyst as supercapacitor electrode, *Ceram. Int.* **44** (2018) 20075-20083.

[5] Y. Zheng, Z. Li, J. Xu, T. Wang, X. Liu, X. Duan, Y. Ma, Y. Zhou, C. Pei, Multi-channeled hierarchical porous carbon incorporated Co_3O_4 nanopillar arrays as 3D binder-free electrode for high performance supercapacitors, *Nano Energy* **20** (2016) 94-107.

[6] D. Bhattacharjya, M.-S. Kim, T.-S. Bae, J.-S. Yu, High performance supercapacitor prepared from hollow mesoporous carbon capsules with hierarchical nanoarchitecture, *J. Power Sources* **244** (2013) 799-805.

[7] L. Mi, W. Wei, S. Huang, S. Cui, W. Zhang, H. Hou, W. Chen, A nest-like Ni@$Ni_{1.4}Co_{1.6}S_2$ electrode for flexible high-performance rolling supercapacitor device design, *J. Mater. Chem. A* **3** (2015) 20973-20982.

[8] M. M. Najafpour, S. I. Allakhverdiev, Manganese compounds as water oxidizing catalysts for hydrogen production via water splitting: From manganese complexes to nano-sized manganese oxides, *Int. J. Hydrog. Energ.* **37** (2012) 8753-8764.

[9] S.-Y. Qi, J. Feng, J. Yan, X.-Y. Hou, M.-L. Zhang, Hydrothermal synthesis and supercapacitor properties of urchin sphere and nanowire MnO_2, *Chin. J. Nonferrous Met.* **18** (2008) 113-117.

[10] K. S. Shaker, A. H. Abdalsalm, Synthesis and characterization nano structure of MnO_2 via chemical method, *Eng. Technol. J.* **36** (2018) 946-950.

[11] K. T. Vadiraj, S. L. Belagali, Photoluminescence behavior of manganese doped zinc sulphide, synthesized by hydrothermal process, *Mater. Today: Proc.* **4** (2017) 11696-11699.

[12] A. K. Worku, D. W. Ayele, N. G. Habtu, Influence of nickel doping on MnO_2 nanoflowers as electrocatalyst for oxygen reduction reaction, *SN Appl. Sci.* **3** (2021) 764.

[13] J. H. Lee, Y. J. Sa, T. K. Kim, H. R. Moon, S. H. Joo, A transformative route to nanoporous manganese oxides of controlled oxidation states with identical textural properties, *J. Mater. Chem. A* **2** (2014) 10435-10443.

[14] N. Swain, A. Mitra, B. Saravanakumar, S. K. Balasingam, S. Mohanty, S. K. Nayak, A. Ramadoss, Construction of three-dimensional MnO_2/Ni network as an efficient electrode material for high performance supercapacitors, *Electrochim. Acta* **342** (2020) 136041.

[15] M. M. L. Sonia, S. Anand, V. M. Vinosel, M. A. Janifer, S. Pauline, Effect of lattice strain on structural, magnetic and dielectric properties of sol–gel synthesized nanocrystalline Ce^{3+} substituted nickel ferrite, *J. Mater. Sci. Mater. Electron.* **29** (2018) 15006-15021.

[16] A. P. Amaliya, S. Anand, S. Pauline, Investigation on structural, electrical and magnetic properties of titanium substituted cobalt ferrite nanocrystallites, *J. Magn. Magn. Mater.* **467** (2018) 14-28.

[17] R. M. Tamgadge, S. Kumar, A. Shukla, A kilohertz frequency response pseudocapacitor, *J. Power Sources* **465** (2020) 228242.

[18] A. Kumar, A. Kumar, A. Kumar, Energy storage properties of double perovskites Gd_2NiMnO_6 for electrochemical supercapacitor application, *Solid State Sci.* **105** (2020) 106252.
[19] K. Wang, B. Lv, Z. Wang, H. Wu, J. Xu, Q. Zhang, Two-fold interpenetrated Mn-based metal-organic frameworks (MOFs) as battery-type electrode materials for charge storage, *Dalton Trans.* **49** (2020) 411-417.